Published in final edited form as:

Brain Struct Funct. 2016 April ; 221(3): 1635–1651. doi:10.1007/s00429-015-0994-y.

Dissociable attentional and inhibitory networks of dorsal and ventral areas of the right inferior frontal cortex: a combined task-specific and coordinate-based meta-analytic fMRI study

Alexandra Sebastian,
Department of Psychiatry and Psychotherapy, Focus Program Translational Neuroscience (FTN), Johannes Gutenberg University Medical Center Mainz, Untere Zahlbacher Str. 8, 55131 Mainz, Germany

Patrick Jung,
Department of Psychiatry and Psychotherapy, Focus Program Translational Neuroscience (FTN), Johannes Gutenberg University Medical Center Mainz, Untere Zahlbacher Str. 8, 55131 Mainz, Germany

Jonathan Neuhoff,
Department of Psychiatry and Psychotherapy, Focus Program Translational Neuroscience (FTN), Johannes Gutenberg University Medical Center Mainz, Untere Zahlbacher Str. 8, 55131 Mainz, Germany

Michael Wibral,
Brain Imaging Center, MEG Unit, Goethe University Frankfurt/Main, Frankfurt/Main, Germany

Peter T. Fox,
Research Imaging Institute, University of Texas Health Science Center, San Antonio, USA

South Texas Veterans Health Care System, San Antonio, USA

Klaus Lieb,
Department of Psychiatry and Psychotherapy, Focus Program Translational Neuroscience (FTN), Johannes Gutenberg University Medical Center Mainz, Untere Zahlbacher Str. 8, 55131 Mainz, Germany

Pascal Fries,
Ernst Strüngmann Institute (ESI) for Neuroscience in Cooperation with Max Planck Society, Frankfurt/Main, Germany

Simon B. Eickhoff,
Institute of Clinical Neuroscience and Medical Psychology, Heinrich-Heine University Düsseldorf, Düsseldorf, Germany

Institute for Neuroscience and Medicine (INM-1), Forschungszentrum Jülich, Jülich, Germany

Correspondence to: Patrick Jung, patrjung@uni-mainz.de.

A. Sebastian, P. Jung, O. Tüscher, A. Mobascher have contributed equally.

Electronic supplementary material The online version of this article (doi:10.1007/s00429-015-0994-y) contains supplementary material, which is available to authorized users.

Oliver Tüscher, and
Department of Psychiatry and Psychotherapy, Focus Program Translational Neuroscience (FTN), Johannes Gutenberg University Medical Center Mainz, Untere Zahlbacher Str. 8, 55131 Mainz, Germany

Departments of Neurology and Psychiatry, Albert-Ludwigs-University Medical Center Freiburg, Freiburg, Germany

Arian Mobascher
Department of Psychiatry and Psychotherapy, Focus Program Translational Neuroscience (FTN), Johannes Gutenberg University Medical Center Mainz, Untere Zahlbacher Str. 8, 55131 Mainz, Germany

Patrick Jung: patrjung@uni-mainz.de

Abstract

The right inferior frontal cortex (rIFC) is frequently activated during executive control tasks. Whereas the function of the dorsal portion of rIFC, more precisely the inferior frontal junction (rIFJ), is convergingly assigned to the attention system, the functional key role of the ventral portion, i.e., the inferior frontal gyrus (rIFG), is hitherto controversially debated. Here, we used a two-step methodical approach to clarify the differential function of rIFJ and rIFG. First, we used event-related functional magnetic resonance imaging (fMRI) during a modified stop signal task with an attentional capture condition (acSST) to delineate attentional from inhibitory motor processes (step 1). Then, we applied coordinate-based meta-analytic connectivity modeling (MACM) to assess functional connectivity profiles of rIFJ and rIFG across various paradigm classes (step 2). As hypothesized, rIFJ activity was associated with the detection of salient stimuli, and was functionally connected to areas of the ventral and dorsal attention network. RIFG was activated during successful response inhibition even when controlling for attentional capture and revealed the highest functional connectivity with core motor areas. Thereby, rIFJ and rIFG delineated largely independent brain networks for attention and motor control. MACM results attributed a more specific attentional function to rIFJ, suggesting an integrative role between stimulus-driven ventral and goal-directed dorsal attention processes. In contrast, rIFG was disclosed as a region of the motor control but not attention system, being essential for response inhibition. The current study provides decisive evidence regarding a more precise functional characterization of rIFC subregions in attention and inhibition.

Keywords

Attentional capture; Functional magnetic resonance imaging; Meta-analytic connectivity modeling; Right inferior frontal cortex; Right inferior frontal junction; Stop signal task

Introduction

The flexible and favorable adaptation of our behavior to changing situations or environments is an important factor of executive control. It is critically dependent on attention steering and motor control. In many circumstances, salient external signals capture our attention and indicate that our ongoing actions or response tendencies need to be stopped and updated.

Response inhibition is required when the goals of our actions are no longer adequate or even harmful.

The functional key role of the right inferior frontal cortex (rIFC) has been differently assigned to both, attentional detection or response inhibition (Aron et al. 2004, 2014; Corbetta and Shulman 2002). It has recently been suggested that those incongruent views might be reconciled by the fact that distinct subregions within the rIFC may be differentially involved in attentional processing and inhibitory motor control (Bari and Robbins 2013; Levy and Wagner 2011). The dorsal part of the rIFC, or more precisely the right inferior frontal junction (IFJ), which is located at the junction of the inferior frontal sulcus and the precentral sulcus (for anatomical details, see Brass et al. 2005; Brass and von Cramon 2002), has quite consistently been linked to attentional processing (Chikazoe et al. 2009; Levy and Wagner 2011; Verbruggen et al. 2010). However, the primary functional role of the ventral part of the rIFC, i.e., the inferior frontal gyrus (rIFG), remains controversial. One line of evidence indicates that the rIFG is a critical node in action updating, which crucially involves response inhibition (Chikazoe et al. 2009; Sebastian et al. 2013; Swick et al. 2011; Verbruggen et al. 2010), while other data suggest a key role in the attentional detection of salient signals (Corbetta et al. 2008; Floden and Stuss 2006; Hampshire et al. 2010; Sharp et al. 2010). It is further possible that the rIFG is essential for both attention and inhibition, i.e., it may relay salient sensory information to facilitate adaptive goal-directed behavior. Finally, rIFG may support multiple cognitive control demands and may thus not be functionally specific to attention and inhibition (Chatham et al. 2012; Duncan 2013; Erika-Florence et al. 2014).

In this study, we aimed (1) at pinpointing the functional assignment of the rIFG to one neural system, i.e., to the motor control or attention system, and (2) at disclosing a more precise functional description of the rIFJ within the attention system. For this purpose, we used a two-step analysis approach: First, we utilized a modified stop signal task version with attentional capture trials (acSST) during event-related functional magnetic resonance imaging (fMRI) to be able to differentiate the task-specific neural networks underlying attentional processing and response inhibition. In a second step, we performed meta-analytic connectivity modeling (MACM) (Eickhoff et al. 2010, 2011; Fox and Lancaster 2002; Laird et al. 2013; Robinson et al. 2010) which is a quantitative coordinate-based meta-analysis over thousands of experiments and healthy subjects. MACM, thus, delineates the neural networks that consistently comprise these rIFC areas under multiple cognitive sets. It hence helps to resolve inconsistencies among the extensive literature of rIFC function which were due to variations in the experimental approaches and their interpretations and designations. Functional characterization of the clusters derived from MACM was performed post hoc to permit taxonomic profiling of brain networks derived in a data-driven fashion in a bottom–up fashion (Eickhoff et al. 2011). This comprised the identification of behavioral domains and paradigm classes to further delineate the functional roles of rIFG and rIFJ and associated brain networks (Laird et al. 2009b).

In line with results from previous studies (Boehler et al. 2011; Cai et al. 2011; Chikazoe et al. 2009), we expected that rIFJ activation is associated with the detection and attentional processing of salient signals. Moreover, we predicted that IFJ co-activates most strongly

with areas of the stimulus-driven ventral attention network (VAN) and/or areas of the goal-directed dorsal attention network (DAN) (Corbetta et al. 2008; Corbetta and Shulman 2002). However, for rIFG, we hypothesized that (1) if it is primarily an attentional area, its task-specific activation behavior and its meta-analytic co-activation pattern would be similar to that of the rIFJ, (2) if it is a genuine motor control area that implements stopping of initiated actions, it should be activated during successful response inhibition and co-activate most strongly with secondary motor areas as well as basal ganglia (Aron 2011), (3) if it is an important relay area integrating the attentional detection of stimulus features with task goals that require inhibition of the initiated action, MACM would reveal a mixed connectivity configuration enclosing areas of both the attention and the motor control network, or (4) if it supports multiple cognitive demands altogether, it should co-active with areas of the so-called multiple-demand brain network (Duncan 2013).

Materials and methods

Participants

Thirty healthy subjects participated in the study. One participant had to be excluded due to excessive head movement (>2 mm) inside the scanner and another one for not following the task instructions. The remaining 28 subjects (11 male) had a mean age of 26.1 years (SD = 5.65, range = 21–47 years). None of the participants took psychotropic medication or had a history or current evidence of a neurological disease. Axis I disorders were excluded by trained psychologists using the Structural Clinical Interview for DSM-IV (SCID-I, First et al. 1996; German version: Wittchen et al. 1997). All subjects gave their written informed consent, were right-handed as determined by the Edinburgh Handedness Inventory (Oldfield 1971) and had normal or corrected to normal vision. The study was approved by the local ethics committee and participants were financially compensated for their time.

Task and procedure

We employed a stop signal task with an attentional control condition (acSST) (Fig. 1) using Presentation software (version 13.0, www.neurobs.com). Before the scanning session, participants received a brief training session on a laptop computer to make sure that the participants correctly understood the task and to familiarize them with the task prior to the scanning session. All subjects accomplished three runs of the acSST during the scanning session. Throughout scanning, participants were asked to hold an MR compatible response button box in their hands and to respond to the stimuli by pressing a response button with the left or right index finger. Prior to the beginning of each run, instructions were given orally. Instructions equally stressed speed and accuracy of responding.

The task comprised three conditions: a go condition (50 %), a stop condition (25 %), and an ac condition (25 %). At the beginning of each trial, a white fixation cross was presented in the center of the screen for 500 ms. Then, a white arrow was displayed for 1,000 ms (equivalent to the maximum permitted reaction time) or until a button press was performed. Subjects were instructed to respond corresponding to the pointing direction of an arrow (i.e., left index finger button press for an arrow pointing to the left and a right index finger button press for an arrow pointing to the right). In the stop condition, the arrow changed its color

from white to blue after a variable stop-signal delay (SSD). Participants were instructed to try canceling the response in case of a stop signal. The SSD was adapted to the participants' performance following a staircase procedure to yield a probability of 50 % of successful response inhibitions per run. The initial SSD was set to 210 ms. If the response was not successfully inhibited (commission error), the SSD in the next stop trial was decreased by 30 ms with a minimum SSD of 40 ms. If a response was successfully inhibited (successful stop), the SSD in the next stop trial was increased by 30 ms. The maximum SSD was limited by the maximum permitted reaction time. In the ac condition, the arrow changed its color from white to green after a variable ac signal delay (ASD) following the onset of the arrow. Participants were instructed to continue their response in case of an ac signal. The ASD was varied in accordance with the staircase in the stop condition. The attribution of color (green/blue) to trial type (stop/ac) was counterbalanced across participants. In case of an omission error (no button press) in the go or ac condition, participants were given a short feedback ("oops—no button press" for 500 ms) to maintain the participants' attention and to limit proactive slowing. The length of the intertrial interval was varied randomly between 2,500 and 3,500 ms. One run consisted of 112 trials presented in a randomized order.

Behavioral data analysis

Behavioral data (reaction time (RT) and accuracy) were collected by the Presentation software, and analyzed using SPSS®, Version 19. Measures of interest were mean RT on correct go and ac trials as well as on failed stop trials, and percentage of commission and omission errors. According to the race model (Logan et al. 1984), the stop-signal reaction time (SSRT) was computed by subtracting the average SSD from the median RT of correct go trials.

Post hoc analysis: selective stopping strategies—It has recently been suggested that participants performing stimulus selective stopping as required in acSSTs may exhibit different selective stopping strategies (Bissett and Logan 2014): (1) If a critical signal is shown (i.e., a blue or green arrow), participants may discriminate the signal before deciding whether or not to stop their response. If the signal is identified as a stop signal, they stop; otherwise they complete the go process without ever initiating the stop process. Hence, RT in ac trials should not be longer compared to go RT. However, as context independence is assumed in this case, RT in incorrect stop trials should be faster compared to go trials (Independent Discriminate then Stop strategy); (2) Participants may inhibit their response upon a critical signal being displayed, and then discriminate the signal to decide whether or not to respond. If the signal is a stop signal, they stop; otherwise they restart the go process. Therefore, RT in ac trials should be longer than in go trials, whereas RT in incorrect stop trials should be faster compared to go trials due to assumed context independence (Stop then Discriminate strategy); (3) The requirement to discriminate stop and ac signals may interact with the go process and slow go RT whenever a critical signal is detected violating the assumptions of the independent race model and resulting in RT in incorrect stop trials which are not shorter than go RT whereas RT in ac trials should be longer than in go trials (Dependent Discriminate then Stop strategy). To classify each participant, we used the procedure described by Bissett and Logan (2014). In short, mean RT for go, ac, and incorrect stop trials were compared for each participant and the implicated strategy was

assigned. To compare the evidence for and against the null hypotheses without bias, Bayes factor, which is the ratio of the odds in favor of the null hypothesis to the odds in favor of the alternative hypothesis, was used (Rouder et al. 2009). When the Bayes factor was greater than 1, we accepted the null hypothesis and when the Bayes factor was less than 1, we accepted the alternative hypothesis (that there was a difference). The Bayes factor was calculated by calculating the mean and standard deviation of go RT, ac RT, incorrect stop RT separately for each participant. Then, go RT and stop RT as well as go RT and ac RT were compared in two independent samples *t* tests. To convert *t* tests and sample sizes to Bayes factors, we used Jeff Rouder's Bayes factor calculator on the Perception and Cognition Lab website (http://pcl.missouri.edu/bf-two-sample) with the recommended Jeffrey-Zellner-Slow Prior with the default value of 1, which is appropriate if there are no strong prior assumptions (Rouder et al. 2009).

MRI data acquisition

Images were acquired on a Magnetom Trio syngo 3 T system (Siemens, Germany), equipped with an 8-channel head coil for signal reception. Stimuli were projected on a screen at the head end of the scanner bore and were viewed with the aid of a mirror mounted on the head coil. Foam padding was used to limit head motion within the coil. A high-resolution T1-weighted anatomical data set was obtained using a 3D magnetization prepared rapid acquisition gradient echo (MPRAGE) sequence for registration purposes (TR = 2,250 ms, TE = 2.6 ms, flip angle = 9°, FOV = 256 mm, 176 sagittal slices, voxel size $1 \times 1 \times 1$ mm^3). Functional MRI images were obtained using T2*-weighted echo-planar imaging (EPI) sequence (TR = 2,500 ms, TE = 30 ms, flip angle = 90°, FOV = 192 mm, 36 slices, voxel size = $3 \times 3 \times 3$ mm^3).

Event-related fMRI data analysis (analysis step 1)

Image preprocessing—SPM8 (www.fil.ion.ucl.ac.uk/spm/software/spm8/) was used to conduct all image preprocessing and statistical analyses, running with Matlab 7.11 (The Mathworks Inc., Natick, Massachusetts, USA). Images were screened for motion artifacts prior to data analysis. Excessive head motion (>2 mm) was observed in one of the participants' who was consequently excluded from all data analyses. Next, images were manually reoriented to the T1 template of SPM. The first five functional images of each run were discarded to allow for equilibrium effects. Then, several preprocessing steps were carried out on the remaining functional images. First, images were realigned to the first image of the first run, using a six degrees-of-freedom rigid body transformation. The realigned functional images were co-registered to the individual anatomical T1 image using affine transformations. Subsequently, using the unified segmentation approach (Ashburner and Friston 2005), the anatomical image was spatially normalized (linear and nonlinear transformations) into the reference system of the Montreal Neurological Institute's (MNI) reference brain using standard templates, and normalization parameters were applied to all functional images. Finally, the normalized functional data were smoothed with a three-dimensional isotropic Gaussian kernel (8 mm fullwidth at half maximum, FWHM) to enhance signal-to-noise ratio and to allow for residual differences in functional neuroanatomy between subjects.

Single subject analysis—A linear regression model (general linear model, GLM) was fitted to the fMRI data of each subject. All events were modeled as stick functions at stimulus onset and convolved with a canonical hemodynamic response function. The model included a high-pass filter with a cut-off period of 128 s to remove drifts or other low-frequency artifacts in the time series. After convolution with a canonical hemodynamic response function, three event types were modeled as regressors of interest: correct reactions for go, stop, and ac trials. Incorrect reactions for each condition and omission error feedback were modeled as regressors of no interest. In addition, the six covariates containing the realignment parameters capturing the subjects' movements during the experiment were included in the model.

Group analysis—The parameter estimates resulting from each condition and subject (first-level analysis) were entered into a second-level, random effects group analysis using a full factorial design. The following contrasts were computed: (1) stop > go; (2) stop > ac; (3) ac > go; (4) ac > stop. Significant effects for each condition were assessed using t statistics. The respective group results were thresholded at $p < 0.05$ corrected for multiple comparisons (family wise error, FWE, correction at voxel level) and $k = 5$ contiguous voxels.

In addition, small volume corrections (SVC) were performed in predefined regions of interest (ROI), i.e. the left and right STN, consisting in a box of $10 \times 10 \times 10$ mm^3 centered at MNI coordinates 10, −15, −5 for right STN and −10, −15, −5 for left STN following Aron and Poldrack (2006). Small volume corrected activations were regarded as significant if they survived $p < 0.05$ for a FWE correction.

To identify regions mutually subserving reactive response inhibition, we conducted a minimum statistic conjunction analysis ('conjunction null'; Nichols et al. 2005) of the contrasts stop > go and stop > ac. This should reveal regions specifically associated with stopping even when contrasted with attentional capture. Regions specifically involved in attentional processing should be significantly activated whenever a salient stimulus would occur irrespective of whether this was a stop signal or an ac signal. To identify regions specifically associated with attentional processing of salient stimuli, we thus performed a conjunction analysis of the contrasts stop > go and ac > go. We expected rIFJ activation to be revealed by this conjunction, as both stop and ac signals are similarly salient and capture attention upon their occurrence. The resulting peak activations within the prefrontal cortex were used as seed regions to the meta-analytic connectivity modeling.

Meta-analytic connectivity modeling (analysis step 2)

Based on the task-specific event-related fMRI results, we performed meta-analytic connectivity modeling (MACM) to delineate consistent functional connectivity profiles of the rIFJ and the rIFG across various paradigm classes and thousands of healthy subjects, making MACM more powerful and reliable than task-specific studies with only a low number of subjects, and enabling brain network analyses in a more general framework.

MACM allows the delineation of cortical networks across databased neuroimaging results by assessing which brain regions show co-activation above chance with a particular seed region in functional neuroimaging experiments independent of the employed paradigm

(Eickhoff et al. 2010, 2011; Laird et al. 2013). Here, spheres with 10 mm in diameter were used as seed masks. The center of the rIFG seed was taken from the conjunction of the stop > go and stop > ac that yielded peak activation in the rIFG region (MNI-coordinates: $x = 42$, $y = 20$, $z = -5$, displayed in red in Fig. 4c). Likewise, the center of the rIFJ seed was based on IFJ peak activity resulting from the conjunction of the contrasts stop > go and ac > go (MNI coordinates: $x = 45$, $y = 8$, $z = 25$, displayed in green in Fig. 4c).

In a first step, all experiments in the BrainMap database, which contained approximately 10,000 neuroimaging experiments at the time of analysis (http://www.brainmap.org; (Fox and Lancaster 2002, Laird et al. 2009a, 2011), were identified that reported stereotaxic coordinates from group analyses of functional mapping experiments of healthy subjects and featured at least one focus of activation in the respective seed. This resulted in approximately 6,500 experiments for analysis. Importantly, all eligible BrainMap experiments were considered independently of the employed paradigm and research questions. This avoided any pre-selection of taxonomic categories which would have constituted a fairly strong a priori hypothesis about how brain networks are organized. We thus opted for a completely data-driven, model-free approach in which experiments were selected exclusively based on the location of their activations. Next, the convergence of foci reported in these experiments was quantified using the revised activation likelihood estimation (ALE) algorithm for coordinate-based meta-analysis of neuroimaging results (Eickhoff et al. 2009; Laird et al. 2009a, b; Turkeltaub et al. 2002) implemented as in-house MATLAB tools. This algorithm aims at identifying regions showing a convergence of reported coordinates across experiments, which is higher than expected under a random spatial association. Importantly, as experiments were defined by activation in the region of interest, the highest convergence will always be found close to the seed. Significant convergence outside the seed, in turn, then indicates functional connectivity over the included numerous experimental tasks (Eickhoff and Grefkes 2011; Jakobs et al. 2012). The key idea behind ALE is to treat the reported foci as centers for 3D Gaussian probability distributions as opposed to single points, capturing the spatial uncertainty associated with each focus. Subsequently, the probability distributions of all foci reported in a given experiment were combined in a non-additive scheme (to prevent summation across foci from the same experiment) into a modeled activation (MA) map (Turkeltaub et al. 2002). The voxel-wise union of these MA maps yielded in voxel-wise ALE scores describing the co-activation probability of that particular location with the current seed voxel. Those ALE scores were then compared to an analytical null distribution reflecting a random spatial association between experiments to statistically test for ‘true’ convergence between studies as opposed to random convergence (i.e., noise) (Eickhoff et al. 2012). A random effects inference is thus invoked, which focuses on inference on the above-chance convergence between studies, in contrast to the clustering of foci within a particular study. The p value of an observed ALE score is given by the proportion of equal or higher values obtained under the null distribution. The ALE maps containing the resulting nonparametric p values for each meta-analysis and reflecting the across-study convergence of co-activation with the seed region were then thresholded at a cluster-level corrected threshold of $p < 0.05$ (cluster-forming threshold at voxel level $p < 0.001$) and transformed into Z-scores for display.

To establish difference maps (contrasts) comparing functional connectivity maps between seeds, we first computed the voxel-wise differences of the ALE scores obtained from the individual MACM analyses. Next, the experiments contributing to either analysis were pooled and subsequently randomly divided into two groups of the same size as the sets of contrasted experiments (Eickhoff and Grefkes 2011). Resulting voxel-wise ALE scores for these two randomly assembled groups were then subtracted from each other and recorded. An empirical null distribution of ALE score differences between the two MACM analyses was obtained by repeating this process 10,000 times. The map of true differences was then thresholded based on this distribution obtained under the null hypothesis of label exchangeability at a posterior probability of $p > 0.95$ for a true difference between the two samples. In other words, using a Monte-Carlo simulation, we identified those voxels in which there was a 95 % confidence for true differences based on a label exchange. The resulting maps were masked with the respective main effect of the minuend connectivity map. This excluded voxels of the difference map that did not show significant co-activation on the underlying connectivity map. In addition, only regions comprising at least 20 cohesive voxels were considered in the resulting difference maps to further protect against incidental findings or edge effects (Rottschy et al. 2013).

Functional characterization of the clusters derived by MACM

Functional characterization of the co-activation-based clusters derived by MACM provides a link between the derived clusters and the putatively corresponding functional differentiation (Eickhoff and Grefkes 2011). The functional characterization of the clusters derived from the MACM was based on the BrainMap meta-data describing the classes of mental processes isolated by the respective statistical contrast of each included experiment. As noted above, it is important to appreciate that we ran MACM without any taxonomic constraints as we opted for a completely data-driven approach in which experiments were exclusively selected based on the location of their activations, only, to delineate genuine brain networks that might be involved in diverse brain functions regardless of the experimental paradigm. The functional characterization was conducted post hoc and independent of the connectivity analysis. Behavioral domains code the mental processes isolated by the statistical contrasts (Fox et al. 2005); these comprise the main categories cognition, action, perception, emotion, and interception, as well as their related sub-categories (i.e., action.inhibition, or cognition.attention). Paradigm classes categorize the specific task employed (i.e., Go/no-go; the complete list of behavioral domains and paradigm classes can be found at http://www.brainmap.org/scribe/).

Functional characterization can be implemented by forward and reverse inference, respectively. Forward inference determines the probability of observing activity in a brain region given knowledge of the psychological process whereas reverse inference assesses the probability of a psychological process being present given knowledge of activation in a specific brain region (Bzdok et al. 2013). For both approaches, we analyzed the behavioral domain and paradigm class meta-data associated with each identified cluster to determine the frequency of its presence within one domain relative to its likelihood across the entire data base. Functional roles of the derived clusters were identified by significant over-representations of behavioral domains and paradigm classes in the experiments revealing

brain activation in one of the respective clusters relative to the BrainMap data base using a binominal test ($p < 0.05$) (Laird et al. 2009b).

Results

Behavioral results

To control for an effect of attribution of color, the experiment was designed in a cross-balanced manner, i.e., the attribution of color (blue/green) to trial type (stop/ac) was balanced across subjects. A two-sample *t* test with color as between factor revealed that the stopping latency as measured by the stop-signal reaction time (SSRT) did not differ significantly between groups ($t_{(28)} = 1.232$, $p = 0.23$). A mixed-design ANOVA with color as between factor and reaction time (RT; go vs. ac) as within factor further revealed no influence of attribution of color to trial type, as no interaction of these two factors was present ($F_{(1,26)} = 1.133$, $p = 0.30$).

Table 1 summarizes behavioral data. Participants performed accurately as indicated in low omission error rates in go and ac trials. Commission error rate of stop trials was close to 50 % indicating the adherence of the subjects to the task rules and the successful operation of the staircase procedure.

A repeated-measures ANOVA based on RT revealed a main effect of condition ($F_{(2,54)} = 176.16$, $p < 0.001$). Bonferroni-corrected post hoc comparisons revealed that RT in ac trials was significantly longer as compared to go trials and failed stop trials (both $p < 0.001$). RT in failed stop trials was significantly shorter as compared to go trials ($p < 0.001$) (Fig. 2a; Table 1). Consistent with the race model assumption of independence of go and stop processes (Logan et al. 1984), neither RT in go nor in ac trials correlated with SSRT (go: $r = -0.017$, $p = 0.93$; ac: $r = -0.116$, $p = 0.56$).

A repeated-measures ANOVA based on accuracy (percentage of correct reactions on go, ac, and stop trials) revealed a main effect of condition ($F_{(2,54)} = 1{,}528.60$, $p < 0.001$). Bonferroni-corrected post hoc comparisons revealed that accuracy in go trials was significantly higher as compared to stop trials ($p < 0.001$), and to ac trials ($p = 0.025$). Accuracy in ac trials was significantly higher as compared to stop trials ($p < 0.001$) (Fig. 2b; Table 1).

Distribution of selective stopping strategies—Following (Bissett and Logan 2014), each participant's selective stopping strategy was classified by comparing their mean go, ac, and incorrect stop RT. We found evidence of the "Independent Discriminate then Stop" strategy in seven of the 28 participants; twelve of the 28 participants could be assigned to the "Stop then Discriminate" strategy; the remaining nine of the 28 participants were classified to use the "Dependent Stop then Discriminate" strategy.

Results of event-related fMRI analysis (analysis step 1)

To identify brain areas involved in successful stopping, in standard SSTs typically the contrast stop > go is used. Importantly, this contrast does not control for attentional processing, as the occurrence of the salient and behaviorally relevant stop signal is likely to

activate both regions associated with attentional and inhibitory processing. Here, the contrast stop > go revealed activation in a bilateral, right lateralized parieto-fronto-striatal network. The cluster in the right inferior frontal cortex showed activation maxima in the rIFG region as well as in the rIFJ (Fig. 3a). Further activation was found in the pre-SMA, the anterior and middle cingulate cortex (ACC and MCC), and bilateral inferior parietal regions. Significant activation (small volume corrected) was also found in the right subthalamic nucleus (STN), and a trend was revealed for the left STN (Table 2).

To control for attentional processing of the stop signal, stop and ac trials were directly contrasted. Stop and ac signals occurred with the same probability and after a matched delay. Hence, both conditions differed only with respect to the stopping demands. The contrast stop > ac, thus, reveals neural correlates specifically associated with successful stopping after controlling for attentional processing and revealed bilateral prefrontal activation. The resulting cluster in the right inferior frontal cortex, however, spanned the rIFG region, only, and did not cover the rIFJ. Further activation was present in the pre-SMA, ACC, and bilateral inferior parietal regions (Fig. 3c, e, g; Table 3).

To test for attentional processing of salient stimuli, the contrast ac > go was used. This resulted in activation in the rIFJ, left dorsolateral prefrontal cortex and bilateral parietal regions. No difference in activation of the rIFG was observed (Fig. 3b, f, h; Table 4).

Contrasting ac > stop revealed activation in bilateral primary sensorimotor regions. This represented most likely the motor response, which was performed during correct ac but not successful stop trials (Fig. 3d; Table 5).

Finally, conjunction analyses further confirmed differential rIFC involvement of rIFJ and rIFG in attentional and inhibitory functioning. The conjunction of the contrasts stop > go and stop > ac which assesses brain regions commonly activated during reactive stopping, revealed activation in bilateral rIFG, SMA, bilateral dorsolateral prefrontal cortex, prefrontal medial cortex as well as in inferior parietal regions (Fig. 3e; Table S1 of Online Resource 1). By contrast, the conjunction of stop > go and ac > go reveals brain regions mutually subserving attentional processing of salient stimuli. This conjunction was associated with activation in the rIFJ and inferior parietal regions (Fig. 3f; Table S2 of Online Resource 2).

Results of MACM analysis (analysis step 2)

MACM (Eickhoff et al. 2010; Fox and Lancaster 2002; Laird et al. 2013; Robinson et al. 2010) is a functional connectivity approach that assesses which brain regions are co-activated above chance with particular seed regions. In the present study, the rIFG, resulting from the contrast stop > ac, and the rIFJ, resulting from the contrast ac > go, were used as seeds. Resulting co-activation patterns were contrasted to assess whether both seeds revealed functional connectivity with distinct networks. The ventral seed (rIFG) showed significantly stronger functional connectivity with a fronto-striatal network related to motor inhibition processes such as the left rIFG, right middle frontal gyrus, pre-SMA, the cerebellum (displayed in red in Fig. 4a) as well as with striatal and subthalamic–thalamic structures (displayed in red in Fig. 4b; Table 6) in direct statistic comparison to the dorsal seed (rIFJ). In contrast, significantly stronger functional connectivity with the dorsal seed (rIFJ) was

found in the left IFJ, bilateral parietal regions and in bilateral temporo-occipital regions (displayed in green in Fig. 4a; Table 7). For the IFJ seed, no significantly stronger co-activation with subcortical regions was found.

Results of functional characterization analysis—Functional characterization of the co-activation patterns with the rIFG and rIFJ, respectively, using the meta-data of the experiments in the BrainMap data confirmed our hypotheses. The functional characterization of the networks resulting from MACM is given in Fig. 5. Across both approaches, forward and reverse inference, the behavioral domains that were significantly associated in the rIFG seed and its associated network were action inhibition and pain perception. As the co-activations of the rIFG covered the anterior insula, the resulting functional assignment of the rIFG to pain perception may be attributable to the fact that the anterior insula is also implicated in pain processing (Treede et al. 2000; Mazzola et al. 2012). Accordingly, rIFG activity was significantly—and primarily—associated with response inhibition paradigms (i.e., Go/no-go tasks) and pain monitor/discrimination paradigms. In addition, it was implicated in spatial/location discrimination tasks and deception paradigms.

The rIFJ and its associated network were most prominently associated with the attentional domain, working memory, action inhibition across both approaches and with language/phonology in the forward inference approach. It is not surprising that the functional characterization of the rIFJ and its associated network revealed inhibition as a functional domain as up to now only few studies have controlled for attentional processing during response inhibition. As rIFJ activity has been linked to attentional processing of stop signals, its activity is usually observed in response inhibition. Paradigm classes most prominently associated with the rIFJ seed comprised mainly working memory and attentional processing tasks in both approaches such as encoding tasks, delayed match to sample paradigms, visual attention/distractor task, or film viewing.

Taken together, the functional characterization further supports the notion of the rIFG and its associated network being mainly implicated in response inhibition, whereas the rIFJ and its associated network are mainly involved in attentional processing.

Discussion

Our two-step methodical approach with (1) task-specific fMRI analyses and (2) data-driven coordinate-based meta-analytic connectivity modeling (MACM) provided strong evidence that the ventral portion of the rIFC (i.e., rIFG) is substantially involved in response inhibition but does not primarily serve the purpose of attentional control, or the integration of attended stimulus features with task goals. The rIFG showed strongest activation during successful response inhibition when contrasted to attentional processing in our acSST task (Fig. 3c, e) and displayed functional connectivity with areas of the motor control network as revealed by MACM (Fig. 4). Moreover, functional characterization of co-activation patterns resulting from MACM (Fig. 5) further corroborates the functional assignment of the rIFG in response inhibition. In contrast, activity of the dorsal portion of the rIFC (i.e., rIFJ) was linked to attention as it was associated with the detection of salient stimuli (Fig. 3b, f, h) and

co-activated most strongly with areas of both the ventral and dorsal attention network (Fig. 4). Its co-activation pattern, as determined by MACM, points at its potential role as a mediator between stimulus-driven ventral and the goal-directed dorsal attention network functions. In addition to clarifying the distinct and precise functional roles of dorsal and ventral portions of the rIFC, we could demonstrate by applying MACM that dorsal and ventral rIFC areas can be employed to delineate largely independent brain networks for attention and response inhibition. Interestingly, the assembly of rIFJ- and rIFG-associated brain networks largely resembles the "canonical" multiple-demand system (Duncan 2013), known to be active in many kinds of complex cognitive tasks. This finding, thus, helps to further differentiate brain network activity that is commonly activated during complex cognition, given that attentional steering and inhibitory control are consistently and crucially involved in complex cognitive tasks.

Task-specific implications

In this well-powered event-related fMRI study, we chose an acSST with a tracking procedure where the SSD was adapted such that the subjects failed to stop their initiated response in 50 % of the stop trials and succeeded to stop in the other 50 % of stop trials. In addition, we yoked the variable signal delays of the ac trials to those of the stop trials to ensure that the contrasts between both trial types were not confounded by differences in stimulus timing. We believe that such a study design is a prerequisite for disentangling attentional and inhibitory processing for the following reasons: In contrast to classical SSTs (e.g., Aron and Poldrack 2006; Sebastian et al. 2013), modified versions of the SST with attentional capture trials (acSST) are needed to dissociate attentional from inhibitory processes. Moreover, event-related fMRI designs and a close proximity of the perceptual properties of stop and ac signals (the only difference: blue vs. green color) are mandatory to accomplish similar attentional processes for stop and ac signals. Most previous studies employing acSSTs used a mixed or block design (Boehler et al. 2011; Cai et al. 2011; Hampshire et al. 2010). However, block designs with stop-relevant vs. stop-irrelevant trials are likely to contrast conditions with large differences in the attentional set and, in turn, the amount of attentional deployment to the salient signals, since they are behaviorally relevant in one block but behaviorally irrelevant in the other. The attentional neglect of salient signals in stop-irrelevant trials would even be a beneficial behavioral strategy, since it prevents the induction of attentional capture processes that potentially interfere with the go process. Moreover, in contrast to event-related designs, block designs are very likely to entail different proactive response strategies, i.e., proactive inhibition will be present during stop-relevant but not stop-irrelevant blocks. As a result, RTs for stop-irrelevant trial blocks are much shorter than for stop-relevant ones (Boehler et al. 2011; Cai et al. 2011). In contrast, RTs of ac trials in our study were significantly longer than RTs of go trials on a group level (but see discussion on individual response strategies below), pointing at the implementation of attentional and discriminative processes in ac trials comparable to stop trials. In other words, behavioral results indicate that subjects envisaged both ac and stop signals as potentially behaviorally relevant, with the only difference that ac and stop signals resumed or initiated the go and stop process, respectively. However, both ac and stop signals, given their perceptual closeness, may initially engage reactive or enhance proactive motor

inhibition and, following discrimination between ac and stop signals, release the motor brake again if ac signals were classified as such (Aron et al. 2014; Bissett and Logan 2014).

The RTs of failed stop trials were significantly shorter than RTs in go trials on a group level. This finding fits well with the independent race model (Logan et al. 1984), which assumes a stochastic and context independence of stop and go processes. In failed stop trials, the go process is faster than the stop process. However, the independent race model does not imply attentional processes although salient signals must first be processed attentionally before goal-directed go or stop processes can be initiated or reactivated. Consequently, failed stop responses might also be due to incomplete attentional processing of the stop signal, resulting in a failed or delayed initiation of the stop process.

However, as recently proposed by Bissett and Logan (2014), selective stopping strategies may vary between subjects and may even lead to a violation of the assumptions of the independent race model. Therefore, the interpretation and comparison of group results or studies which most probably present a mixture of those selective stopping strategies have to be seen with caution and may heavily depend on the proportion of subjects using one or the other strategy.

Task-specific activation patterns of rIFC

Results of analysis step 1 (task-specific event-related fMRI analysis) showed that the dorsal rIFC, more specifically the rIFJ, was activated whenever a salient stimulus was presented, irrespective of whether this was a stop or ac stimulus (Fig. 3a, b, e). This indicates that the rIFJ subserves bottom–up attentional processing of salient stimuli, which is in line with previous studies using response inhibition tasks with ac trials (Boehler et al. 2011; Cai et al. 2011; Chikazoe et al. 2009). Other lines of research have linked rIFJ activation to a broad range of cognitive control tasks, such as task switching, n-back, and Stroop paradigms (Derrfuss et al. 2012) usually involving heightened attentional processing.

A recent meta-analysis (Levy and Wagner 2011) revealed that the rIFJ does not simply respond to infrequent events but is specifically associated with the detection of behaviorally relevant stimuli. The results of the present study are well in line with these findings. RIFJ activation was stronger during stop than ac trials (Fig. 3h). Even though this difference was not statistically significant, it corroborates the notion of the rIFJ responding stronger to behaviorally relevant signals that require a change of the current behavior, i.e., action updating, than to those that do not require a change of the ongoing action (Chan and Downing 2011; Downar et al. 2001; Levy and Wagner 2011).

Ventral rIFC activation, more specifically the rIFG, was primarily associated with successful response inhibition in the present study as revealed by contrasting stop to go as well as to ac trials (Fig. 3a, c) or the conjunction of these contrasts (Fig. 3e). In addition, rIFG activity was absent when contrasting ac to go trials indicating that the rIFG is critically involved in response inhibition but not in the detection of salient and behaviorally relevant stimuli. Of note, these results are at variance with those of the only previously published study (Sharp et al. 2010) that is methodologically comparable with our analysis step 1 procedure, i.e., event-related fMRI analysis was used for an acSST in an event-related design. Sharp et al. (2010)

reported that only the pre-SMA but not the rIFG showed significant activation in the contrast stop > ac. However, according to the selective stopping strategies proposed by Bissett and Logan (2014), they calculated that only 23 % of subjects in the study of Sharp et al. (2010) employed the stop then discriminate strategy, whereas this was the case for 43 % in our study, as assessed in a post hoc analysis. Moreover, 23 % of the participants could not be assigned to any of the proposed strategies in the study by Sharp et al. (2010). Part of the reason for the discrepant results may thus lie in the different selective stopping strategies of most subjects in Sharp's and our study and the associated different weightings of discrimination and stop processes. Unfortunately, subgroups of our sample assigned to one of the selective stopping strategies were too small for a valid subgroup comparisons of the functional imaging data.

While there are a few other studies that assign a pivotal attentional but not inhibitory role to the rIFG (Hampshire et al. 2010; Tabu et al. 2011), most investigations employing response inhibition tasks with ac trials are in line with our results (Boehler et al. 2011; Cai et al. 2011, Chikazoe et al. 2009). Thereby, the only event-related fMRI study that used a Go/No-Go task with intermingled ac trials (Chikazoe et al. 2009) showed findings that closely resemble the current results, although stop signal and go/no-go tasks capture different subcomponents of response inhibition (Sebastian et al. 2013; Swick et al. 2011).

As discussed earlier, ac signals in our study may initially drive some inhibitory motor processing due to their perceptual proximity to the stop signals. This would result in some initial inhibitory activation for the contrast ac vs. go and might overall result in slightly reduced inhibitory activity for the contrast stop vs. ac. With regard to rIFG activation, our results were at least not relevantly distorted by such conceivable effects, since rIFG showed no activity in the contrast ac > go but strong activation for stop > ac. For rIFJ activation, however, event-related fMRI results (analysis step 1) cannot rule out that some portion of activity seen in the contrast ac > go reflect inhibitory processing. Yet the meta-analytic brain network analysis, as conducted in analysis step 2 and discussed in the next paragraph, gave further insight into the exact function of rIFJ.

Coordinate-based MACM co-activation patterns of rIFC

Results from the event-related fMRI analysis suggested that the rIFJ is primarily responsible for attentional processing of salient signals whereas the rIFG is essential for response inhibition. However, these results are specific for the experimental setup, the task (acSST) and the dominant selective stopping strategy. To detect the functional connectivity pattern of the ROIs within rIFC that were identified in the initial analysis step with a maximum level of generalizability, robustness, and power, we performed MACM (Eickhoff et al. 2010; Fox and Lancaster 2002; Laird et al. 2013; Robinson et al. 2010) for rIFJ and rIFG in a second analysis step, i.e., we identified the functional connectivity of these areas across thousands of subjects and various paradigm classes.

For rIFJ, MACM revealed the strongest functional connectivity with the left IFJ, bilateral parietal regions and bilateral temporo-occipital regions (Fig. 4a, green color), i.e., regions of the attention network. Interestingly, the co-activation pattern of rIFJ resulting from MACM comprised both areas of the ventral and the dorsal attention network (cf. Corbetta et al.

2008). This implies that the rIFJ is a key region within the attentional system. If rIFJ was primarily responsible for stimulus-driven attentional processes, then it would co-activate most strongly with VAN areas, such as the inferior parietal lobule, the lateral occipital cortex, the temporoparietal junction and the ventral frontal cortex, including parts of middle frontal cortex and inferior frontal cortex; if rIFJ was essential for goal-directed attentional processes only, it would show the closest functional linkage with DAN areas, such as the intraparietal sulcus, the superior parietal lobule, the frontal cortex near or at the frontal eye field and higher-order visual areas (V4, MT). Yet the functional connectivity of rIFJ with both ventral and dorsal attention network areas points at its potential role as a mediator between stimulus-driven VAN and goal-directed DAN functions. In accordance, Corbetta et al. (2008) attributed the same function to an area that is identical or at least in very close proximity to our rIFJ location. Moreover, Levy and Wagner (2011) suggested that the rIFJ might mediate the interaction between stimulus-driven and goal-directed attentional processes. The present results are in line with these conjectures.

For rIFG, MACM determined the strongest functional connections to the left IFG/Ins, right middle frontal gyrus, pre-SMA, SMA, the cerebellum (Fig. 4a, red color), as well as with striatal and subthalamic-thalamic structures (Fig. 4b, red color). Hence, rIFG showed the closest functional connectivity with motor control areas but, in contrast to rIFJ, not with parietal and occipital areas that serve visual attentional functions. This points to a genuine motor control function of the rIFG. While also taking into account the results of step 1 (event-related fMRI analysis), it must be assumed that rIFG is of crucial importance for motor inhibition, a prerequisite of action updating. The MACM functional connectivity configuration of rIFG, however, did not imply ventral or dorsal network areas, making a primary attentional function unlikely. Moreover, MACM co-activation patterns of rIFG did not demonstrate a mixture of both attentional and motor network regions, arguing against an intermediary role between attentional and motor functions.

Recent publications investigated the rIFC in multiple executive tasks and concluded that primary rIFC functions cannot be considered as top–down inhibitory control anymore but as essential for more general cognitive demands, such as context-monitoring (Chatham et al. 2012) or construction of attentional episodes (Duncan 2013), potentially through a basic top–down potentiation mechanism (Erika-Florence et al. 2014). However, our MACM data partly counter this notion and argue for a primary role of ventral rIFG in action updating including motor inhibition (Verbruggen et al. 2010), since it is functionally connected to core regions of the motor system or more generally speaking of the fronto-striatal system, only. The dominant linkage of rIFG with the fronto-striatal motor system was further corroborated by its dominant association with the behavioral domain ‘action inhibition’ and go/no-go-related paradigms. The rIFG seed for MACM partially incorporated the anterior insula, known for its importance in pain processing (Treede et al. 2000; Mazzola et al. 2012), which explains its additional significant functional linkage to the behavioral domain ‘Perception. Somethesis. Pain’ and pain discrimination paradigms where it as well may execute inhibitory control over pain perception.

Duncan (2013) identified ubiquitous brain activity across many cognitive domains. This multiple-demand system compromised bilateral activity of the IFJ, IFG, anterior insula,

dorsolateral PFC, dorsal anterior cingulate, pre-SMA, premotor cortex, intraparietal sulcus, higher visual areas (in visual tasks), cerebellum, thalamus und basal ganglia. In this study, left IFJ, dorsal anterior cingulate, premotor cortex, intraparietal sulcus and higher visual areas represented the rIFJ-associated MACM network, whereas rIFG was co-activated with left IFG, anterior insula, dorsolateral PFC, pre-SMA, premotor cortex, cerebellum, thalamus und basal ganglia. Thus, the merge of rIFJ- and rIFG-associated network areas largely resembles the multiple-demand system. Intriguingly, the dissociation suggested by our study into an attentional, dorso-parietal and inhibitory, ventro-frontal-striatal network fits the idea of attention and inhibition as central processes within the executive system providing the basis for performance monitoring and action selection, respectively, allowing the brain to perform action updating and shifting (Bari and Robbins 2013; Levy and Wagner 2011).

Conclusions and significance

The present study gives important insights into the precise function of dorsal and ventral portions of the rIFC. Previous evidence already suggested a general importance of rIFJ (dorsal part of rIFC) for attentional processes but the exact functional role of rIFJ within the attentional system remained to be elucidated. In this study, task-specific BOLD contrast fMRI analysis confirmed the importance of rIFJ for attentional processing of salient external signals. However, MACM analysis enabled a closer assignment of rIFJ function since its co-activation with both DAN and VAN areas implies that rIFJ relays top–down signals from DAN to VAN areas, e.g., to restrict VAN activation to behaviorally relevant stimuli. With respect to rIFG (ventral part of rIFC), task-specific fMRI and coordinate-based MACM results clearly disclosed a genuine motor control function. More specifically, they suggest that rIFG is crucially involved in response inhibition as a part of an action selection and updating system. Hence, rIFJ- and rIFG-dissociated brain networks may constitute attentional and inhibitory core systems of executive functioning (Bari and Robbins 2013) and act in concert to enable executive functioning in general (Bari and Robbins 2013; Duncan 2013). Together, the assembly of rIFJ- and rIFG-associated brain networks forms a network which largely resembles the multiple-demand system, ubiquitously active during many executive control tasks (Duncan 2013). Thus, the delineated, distinctive attentional and inhibitory networks of dorsal and ventral rIFC subregions are potentially relevant for future studies on executive control, in particular for investigations of subjects with impulse control deficits.

Supplementary Material

Refer to Web version on PubMed Central for supplementary material.

Acknowledgments

This work was supported by internal grants of the MAIFOR program and the research focus translational neurosciences (FTN) of the Johannes Gutenberg University Medical Center Mainz, Germany. Comprehensive access to the BrainMap database was authorized by a collaborative-use license agreement, provided to Simon Eickhoff by the University of Texas Health Science Center at San Antonio. BrainMap is supported by NIH/NIMH R01 MH074457. Findings presented in this study are part of the doctoral thesis of Jonathan Neuhoff.

References

Aron AR. From reactive to proactive and selective control: developing a Richer Model for stopping inappropriate responses. Biol Psychiatry. 2011; 69:e55–e68. [PubMed: 20932513]

Aron AR, Poldrack RA. Cortical and subcortical contributions to stop signal response inhibition: role of the subthalamic nucleus. J Neurosci. 2006; 26:2424–2433. [PubMed: 16510720]

Aron AR, Robbins TW, Poldrack RA. Inhibition and the right inferior frontal cortex. Trends Cogn Sci. 2004; 8:170–177. [PubMed: 15050513]

Aron AR, Robbins TW, Poldrack RA. Inhibition and the right inferior frontal cortex: one decade on. Trends Cogn Sci. 2014; 18(4):177–185.10.1016/j.tics.2013.12.003 [PubMed: 24440116]

Ashburner J, Friston KJ. Unified segmentation. NeuroImage. 2005; 26:839–851. [PubMed: 15955494]

Bari A, Robbins TW. Inhibition and impulsivity: behavioral and neural basis of response control. Prog Neurobiol. 2013; 108:44–79. [PubMed: 23856628]

Bissett PG, Logan GD. Selective stopping? Maybe not. J Exp Psychol Gen. 2014; 143:455–472. [PubMed: 23477668]

Boehler CN, Appelbaum LG, Krebs RM, Chen L, Woldorff MG, Wenderoth N. The role of stimulus salience and attentional capture across the neural hierarchy in a stop-signal task. PLoS One. 2011; 6:e26386. [PubMed: 22022611]

Brass M, von Cramon DY. The role of the frontal cortex in task preparation. Cereb Cortex. 2002; 12:908–914. [PubMed: 12183390]

Brass M, Ullsperger M, Knoesche TR, von Cramon DY, Phillips NA. Who comes first? The role of the prefrontal and parietal cortex in cognitive control. J Cogn Neurosci. 2005; 17:1367–1375. [PubMed: 16197690]

Bzdok D, Langner R, Schilbach L, Jakobs O, Roski C, Caspers S, Laird AR, Fox PT, Zilles K, Eickhoff SB. Characterization of the temporo-parietal junction by combining data-driven parcellation, complementary connectivity analyses, and functional decoding. Neuroimage. 2013; 81:381–392. [PubMed: 23689016]

Cai W, Leung H, Greenlee MW. Rule-guided executive control of response inhibition: functional topography of the inferior frontal cortex. PLoS One. 2011; 6:e20840. [PubMed: 21673969]

Chan AW, Downing PE. Faces and eyes in human lateral prefrontal cortex. Front Hum, Neurosci. 2011; 5

Chatham CH, Claus ED, Kim A, Curran T, Banich MT, Munakata Y. Cognitive control reflects context monitoring, not motoric stopping, in response inhibition. PLoS One. 2012; 7(2):e31546. [PubMed: 22384038]

Chikazoe J, Jimura K, Asari T, Yamashita K, Morimoto H, Hirose S, Miyashita Y, Konishi S. Functional dissociation in right inferior frontal cortex during performance of go/no-go task. Cereb Cortex. 2009; 19:146–152. [PubMed: 18445602]

Corbetta M, Shulman GL. Control of goal-directed and stimulus-riven attention in the brain. Nat Rev Neurosci. 2002; 3:215–229.

Corbetta M, Patel G, Shulman GL. The Reorienting system of the human brain: from environment to theory of mind. Neuron. 2008; 58:306–324. [PubMed: 18466742]

Derrfuss J, Vogt V, Fiebach C, von Cramon D, Tittgemeyer M. Functional organization of the left inferior precentral sulcus: dissociating the inferior frontal eye field and the inferior frontal junction. NeuroImage. 2012; 59:3829–3837. [PubMed: 22155041]

Downar J, Crawley AP, Mikulis DJ, Davis KD. The effect of task relevance on the cortical response to changes in visual and auditory stimuli: an event-related fMRI study. Neuroimage. 2001; 14:1256–1267. [PubMed: 11707082]

Duncan J. The structure of cognition: attentional episodes in mind and brain. Neuron. 2013; 80(1):35–50. [PubMed: 24094101]

Eickhoff SB, Grefkes C. Approaches for the integrated analysis of structure, function and connectivity of the human brain. Clin EEG Neurosci. 2011; 42:107–121. [PubMed: 21675600]

Eickhoff SB, Laird AR, Grefkes C, Wang LE, Zilles K, Fox PT. Coordinate-based activation likelihood estimation meta-analysis of neuroimaging data: a random-effects approach based on empirical estimates of spatial uncertainty. Hum Brain Mapp. 2009; 30:2907–2926. [PubMed: 19172646]

Eickhoff SB, Jbabdi S, Caspers S, Laird AR, Fox PT, Zilles K, Behrens TEJ. Anatomical and functional connectivity of cytoarchitectonic areas within the human parietal operculum. J Neurosci. 2010; 30:6409–6421. [PubMed: 20445067]

Eickhoff SB, Bzdok D, Laird AR, Roski C, Caspers S, Zilles K, Fox PT. Co-activation patterns distinguish cortical modules, their connectivity and functional differentiation. Neuroimage. 2011; 57:938–949. [PubMed: 21609770]

Eickhoff SB, Bzdok D, Laird AR, Kurth F, Fox PT. Activation likelihood estimation meta-analysis revisited. Neuroimage. 2012; 59:2349–2361. [PubMed: 21963913]

Erika-Florence M, Leech R, Hampshire A. A functional network perspective on response inhibition and attentional control. Nature Commun. 2014; 5:4073. [PubMed: 24905116]

First, M.; Spitzer, R.; Gibbon, M.; Williams, J. Structured Clinical interview for DSM-IV axis I disorders, clinician version (SCID-CV). American Psychiatric Press Inc; Washington, DC: 1996.

Floden D, Stuss DT. Inhibitory control is slowed in patients with right superior medial frontal damage. J Cogn Neurosci. 2006; 18:1843–1849. [PubMed: 17069475]

Fox PT, Lancaster JL. Opinion: mapping context and content: the BrainMap model. Nat Rev Neurosci. 2002; 3:319–321. [PubMed: 11967563]

Fox PT, Laird AR, Fox SP, Fox PM, Uecker AM, Crank M, Koenig SF, Lancaster JL. BrainMap taxonomy of experimental design: description and evaluation. Hum Brain Mapp. 2005; 25:185–198. [PubMed: 15846810]

Hampshire A, Chamberlain SR, Monti MM, Duncan J, Owen AM. The role of the right inferior frontal gyrus: inhibition and attentional control. NeuroImage. 2010; 50:1313–1319. [PubMed: 20056157]

Jakobs O, Langner R, Caspers S, Roski C, Cieslik EC, Zilles K, Laird AR, Fox PT, Eickhoff SB. Across-study and within-subject functional connectivity of a right temporo-parietal junction subregion involved in stimulus–context integration. NeuroImage. 2012; 60:2389–2398. [PubMed: 22387170]

Laird AR, Eickhoff SB, Kurth F, Fox PM, Uecker AM, Turner JA, Robinson JL, Lancaster JL, Fox PT. ALE meta-analysis workflows via the brainmap database: progress towards a probabilistic functional brain atlas. Front Neuroinform. 2009a; 3:23. [PubMed: 19636392]

Laird AR, Eickhoff SB, Li K, Robin DA, Glahn DC, Fox PT. Investigating the functional heterogeneity of the default mode network using coordinate-based meta-analytic modeling. J Neurosci. 2009b; 29:14496–14505. [PubMed: 19923283]

Laird AR, Eickhoff SB, Fox PM, Uecker AM, Ray KL, Saenz JJ, McKay DR, Bzdok D, Laird RW, Robinson JL, Turner JA, Turkeltaub PE, Lancaster JL, Fox PT. The BrainMap strategy for standardization, sharing, and meta-analysis of neuroimaging data. BMC Res Notes. 2011; 4:349. [PubMed: 21906305]

Laird AR, Eickhoff SB, Rottschy C, Bzdok D, Ray KL, Fox PT. Networks of task co-activations. NeuroImage. 2013; 80:505–514. [PubMed: 23631994]

Levy BJ, Wagner AD. Cognitive control and right ventrolateral prefrontal cortex: reflexive reorienting, motor inhibition, and action updating. Ann N Y Acad Sci. 2011; 1224:40–62. [PubMed: 21486295]

Logan GD, Cowan W, Davis K. On the ability to inhibit responses in simple and choice reaction time tasks: a model and a method. J Exp Psychol Hum Percept Perform. 1984; 10(2):276–291. [PubMed: 6232345]

Mazzola L, Faillenot I, Barral FG, Mauguiere F, Peyron R. Spatial segregation of somato-sensory and pain activations in the human operculo-insular cortex. Neuroimage. 2012; 60(1):409–418. [PubMed: 22245639]

Nichols T, Brett M, Andersson J, Wager T, Poline JB. Valid conjunction inference with the minimum statistic. NeuroImage. 2005; 25:653–660. [PubMed: 15808966]

Oldfield RC. The assessment and analysis of handedness: the Edinburgh inventory. Neuropsychologia. 1971; 9:97–113. [PubMed: 5146491]

Robinson JL, Laird AR, Glahn DC, Lovallo WR, Fox PT. Metaanalytic connectivity modeling: delineating the functional connectivity of the human amygdala. Hum Brain Mapp. 2010; 31:173–184. [PubMed: 19603407]

Rottschy C, Caspers S, Roski C, Reetz K, Dogan I, Schulz JB, Zilles K, Laird AR, Fox PT, Eickhoff SB. Differentiated parietal connectivity of frontal regions for "what" and "where" memory. Brain Struct Funct. 2013; 218(6):1551–1567.10.1007/s00429-012-0476-4 [PubMed: 23143344]

Rouder JN, Speckman PL, Sun D, Morey RD, Iverson G. Bayesian *t* tests for accepting and rejecting the null hypothesis. Psychon Bull Rev. 2009; 16(2):225–237.10.3758/PBR.16.2.225 [PubMed: 19293088]

Sebastian A, Pohl M, Klöppel S, Feige B, Lange T, Stahl C, Voss A, Klauer K, Lieb K, Tüscher O. Disentangling common and specific neural subprocesses of response inhibition. NeuroImage. 2013; 64:601–615. [PubMed: 22986077]

Sharp DJ, Bonnelle V, de Boissezon X, Beckmann CF, James SG, Patel MC, Mehta MA. Distinct frontal systems for response inhibition, attentional capture, and error processing. Proc Natl Acad Sci USA. 2010; 107:6106–6111. [PubMed: 20220100]

Swick D, Ashley V, Turken U. Are the neural correlates of stopping and not going identical? Quantitative meta-analysis of two response inhibition tasks. NeuroImage. 2011; 56:1655–1665. [PubMed: 21376819]

Tabu H, Mima T, Aso T, Takahashi R, Fukuyama H. Functional relevance of pre-supplementary motor areas for the choice to stop during Stop signal task. Neurosci Res. 2011; 70:277–284. [PubMed: 21440014]

Treede RD, Apkarian AV, Bromm B, Greenspan JD, Lenz FA. Cortical representation of pain: functional characterization of nociceptive areas near the lateral sulcus. Pain. 2000; 87(2):113–119. [PubMed: 10924804]

Turkeltaub PE, Eden GF, Jones KM, Zeffiro TA. Meta-analysis of the functional neuroanatomy of single-word reading: method and validation. Neuroimage. 2002; 16:765–780. [PubMed: 12169260]

Verbruggen F, Aron AR, Stevens MA, Chambers CD. Theta burst stimulation dissociates attention and action updating in human inferior frontal cortex. Proc Natl Acad Sci USA. 2010; 107:13966–13971. [PubMed: 20631303]

Wittchen, H.; Wunderlich, U.; Gruschwitz, S.; Zaudig, M. Achse I: Psychische Störungen. Göttingen: Hogrefe; 1997. SKID-I. Strukturiertes Klinisches Interview für DSM-IV.

Fig. 1.

Stop signal task with attentional capture (ac)-trials. Participants were instructed to press a button corresponding to the pointing direction of an *arrow* (go trials). In stop trials, the *arrow* changed its *color* from *white* to *blue* after a variable stop-signal delay (SSD) indicating that the participants should cancel the response. In ac trials, the arrow changed its *color* from *white* to *green* after a variable ac signal delay (ASD). Participants were instructed to continue their response in ac trials. The attribution of color (*green*/*blue*) to trial type (stop/ac) was counterbalanced across participants

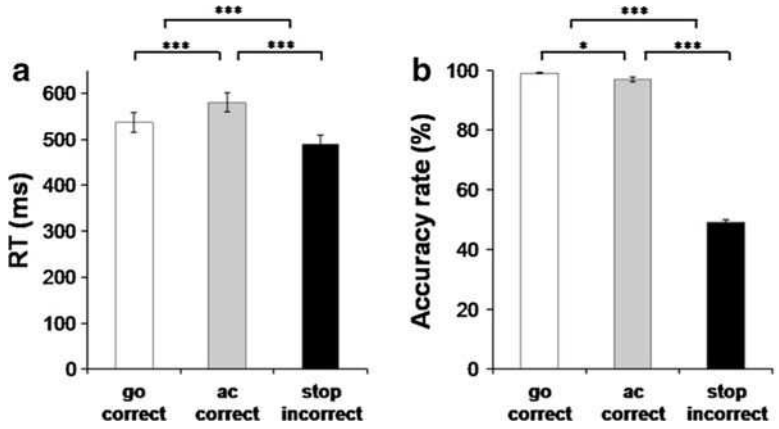

Fig. 2.

Behavioral data during performance of the stop signal task (mean ± standard error of the mean). **a** Reaction time (RT) in correct go, correct attentional capture (ac), and failed stop trials, and **b** performance in correct go, correct ac, and successful stop trials are displayed. ***$p < 0.001$, *$p < 0.05$ based on Bonferroni-corrected post hoc comparisons of a repeated-measures ANOVA. Note that RT in ac trials was significantly longer as compared to go trials presumably reflecting attentional processing. Commission error rate of stop trials was close to 50 % indicating the success of the staircase procedure

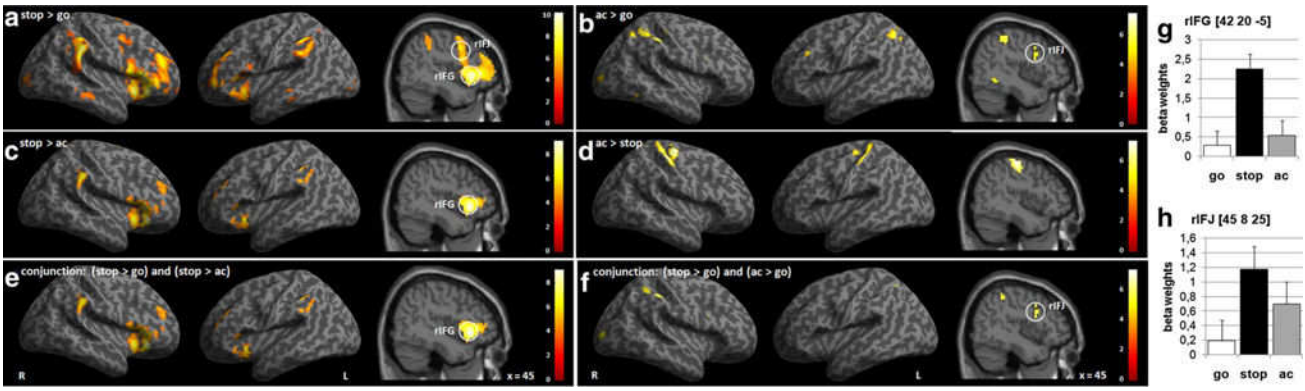

Fig. 3.

Activation maps for the contrasts **a** stop–go; **b** attentional capture (ac)–go; **c** stop–ac; **d** ac–stop; **e** conjunction of the contrasts (stop–go) and (stop–ac); **f** conjunction of the contrasts (stop–go) and (ac–go). All maps are thresholded at pFWE <0.05, cluster extent $k = 5$ voxel). The color scale represents *t*-scores. Beta-weights have been extracted for peak activation in **g** right inferior frontal gyrus (rIFG), and **h** right inferior frontal junction (IFJ). Note that rIFG activity is present during stopping (**a**), even after controlling for attentional processing (**c, e**), whereas IFJ activity is present during attentional processing of stop and ac signals (**a, b, f**)

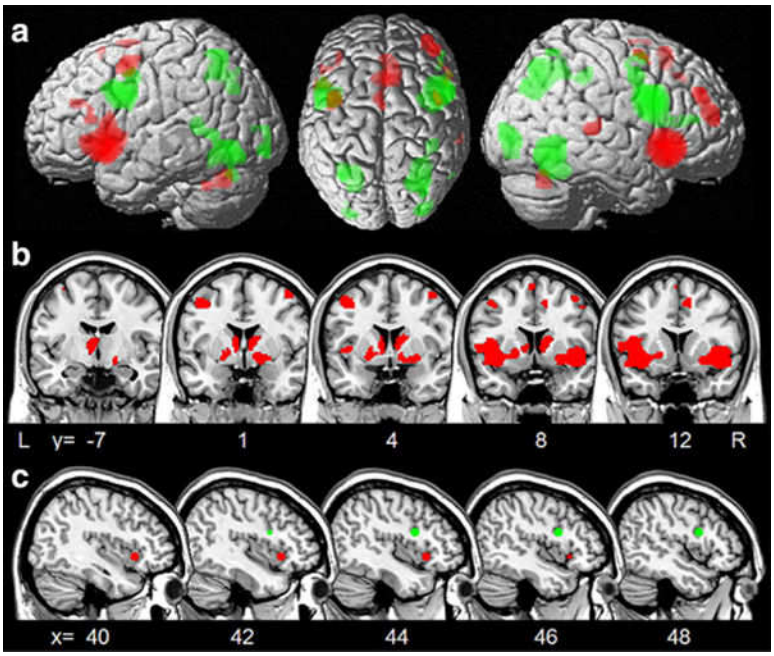

Fig. 4.

Significant differences in connectivity patterns in **a** cortical and **b** subcortical structures. Regions showing stronger co-activation with the right inferior frontal gyrus (rIFG) are illustrated in *red*, while regions showing stronger co-activation with the right inferior frontal junction (rIFJ) are shown in *green*. Note that rIFG is closely linked to areas of the motor control network, whereas rIFJ is connected to key areas of the visual attention network. **c** Seeds that were used for the meta-analytic connectivity modeling approach. rIFG (*red*, MNI-coordinates: $x = 42$, $y = 20$, $z = -5$); rIFJ (*green*, MNI-coordinates: $x = 45$, $y = 8$, $z = 25$)

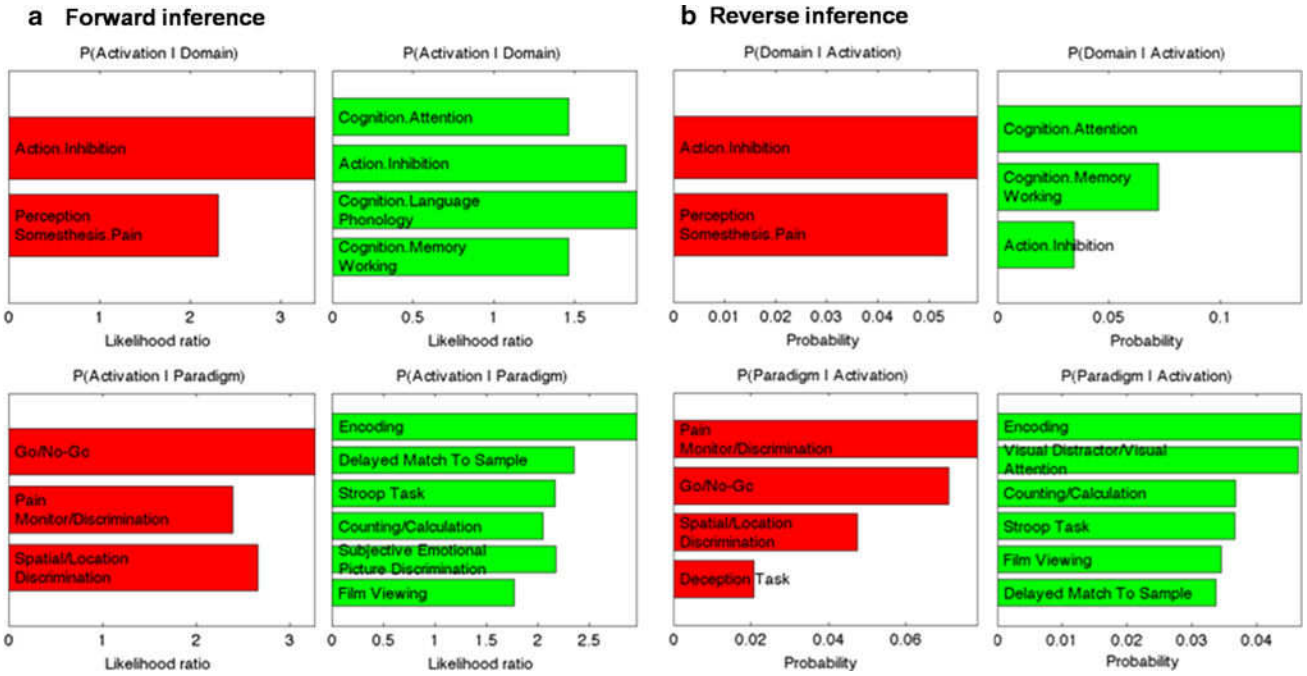

Fig. 5.

Domain and paradigm associations of the rIFG (*red*) and the rIFJ (*green*). BrainMap meta-data were used to perform functional forward (**a**) and reverse (**b**) inference for both clusters. Behavioral domains are shown on *top*, paradigm classes on the *bottom*. Forward inference tests above-chance brain activity given the presence of a psychological process, whereas reverse inference tests the above-chance probability of a term given observed brain activity

Table 1

Behavioral results

Behavioral measure		
Median RT go (ms)	529.6	±116.3
Median RT ac (ms)	576.9	±123.1
Median RT failed stop (ms)	489.4	±103.4
Omission errors go (%)	0.9	±1.3
Omission errors ac (%)	3.1	±4.2
Commission errors stop (%)	49.3	±4.3
SSRT (ms)	251.2	±30.9
SSD (ms)	278.4	±120.9

SSRT is calculated by subtracting the mean stop-signal delay from the median RT (go). Percentage error is estimated by dividing the number of incorrect go/ac trials (omissions)/stop trials (commissions) by the total number of the trial type

RT reaction time, *ac* attentional capture, *SSRT* stop-signal reaction time, *SSD* stop-signal delay

Table 2

Activation foci for the contrast stop > go

Region		*x*	*y*	*z*	*Z*	*p*	*k*
Prefrontal cortex							
Insula lobe, inferior frontal gyrus (p. Triangularis, p. Opercularis), middle frontal gyrus	R	42	20	−5	Inf	<0.001	1,378
Insula lobe, inferior frontal gyrus (p. Triangularis, p. Opercularis)	L	−33	20	−5	6.78	<0.001	375
Inferior frontal gyrus (p. Triangularis), middle frontal gyrus	L	−45	47	4	6.59	<0.001	281
Pre-SMA	R	15	2	67	6.29	<0.001	64
Middle cingulate cortex, anterior cingulate cortex, superior medial gyrus	R	6	26	40	5.81	<0.001	231
Middle cingulate cortex	R	0	−22	31	5.25	0.002	21
Parietal cortex							
Supra marginal gyrus, inferior parietal lobule, superior temporal gyrus, middle temporal gyrus	R	63	−37	37	7.60	<0.001	426
Inferior parietal lobule, Temporal and occipital cortex	L	−63	−43	40	7.67	<0.001	265
Middle temporal gyrus, middle occipital gyrus	R	63	−31	−11	5.34	0.001	55
Subcortical areas							
Striatum	R	12	8	1	5.75	<0.001	64
Striatum	L	−12	8	1	5.27	0.001	24
Subthalamic nucleus	R	9	−13	−2	2.99	0.019[a]	19
Subthalamic nucleus	L	−6	−13	−2	2.60	0.051[a]	13

Local maxima of brain activations during successful stop–go in Montreal Neurological Institute (MNI) *x*-, *y*-, and *z*-coordinates with associated *Z*-score ($p_{FWE} < 0.05$) and cluster extent in number of voxel (k)

Pre-SMA pre-supplemental motor area, *R* right, *L* left

[a] small volume corrected

Table 3

Activation foci for the contrast stop > attentional capture

Region		*x*	*y*	*z*	*Z*	*p*	*k*
Prefrontal cortex							
Insula lobe	R	42	20	−5	7.65	<0.001	582
Insula lobe	L	−33	20	−5	6.10	<0.001	240
Middle frontal gyrus	R	33	50	25	5.53	<0.001	100
Middle frontal gyrus	L	−39	44	28	5.83	0.001	59
Superior medial gyrus, anterior cingulate cortex	L	−3	38	31	4.88	0.009	47
Pre-SMA	R	15	−1	67	5.32	0.001	11
Middle cingulate cortex	R	6	26	40	4.63	0.026	6
Superior frontal gyrus	R	18	17	61	4.77	0.014	5
Parietal cortex							
Supra marginal gyrus	R	63	−43	31	6.48	<0.001	125
Inferior parietal lobule	L	−57	−46	49	6.32	<0.001	115
Inferior parietal lobule	L	−54	−49	52	5.77	<0.001	–

Local maxima of brain activations during successful stop—attentional capture (ac) in Montreal Neurological Institute (MNI) *x*-, *y*-, and *z*-coordinates with associated *Z*-score (p_{FWE}<0.05) and cluster extent in number of voxel (*k*)

Pre-SMA pre-supplemental motor area, *R* right, *L* left

Table 4

Activation foci for the contrast attentional capture > go

Region		*x*	*y*	*z*	*Z*	*p*	*k*
Prefrontal cortex							
Middle frontal gyrus	L	−48	29	31	5.03	0.004	15
Inferior frontal gyrus (p. Opercularis)	R	45	8	25	4.86	0.014	13
Middle frontal gyrus	R	45	8	40	4.74	0.016	5
Parietal cortex							
Inferior parietal lobule	R	54	−31	52	6.53	<0.001	191
Superior parietal lobule	L	−30	−61	46	5.76	<0.001	70
Inferior parietal lobule	L	−48	−40	52	4.94	0.007	24
Temporal and occipital cortex							
Middle occipital gyrus	R	30	−88	7	4.91	0.008	19
Inferior temporal gyrus	R	51	−52	−11	4.77	0.014	18

Local maxima of brain activations during successful stop—attentional capture (ac) in Montreal Neurological Institute (MNI) *x*-, *y*-, and *z*-coordinates with associated *Z*-score (p_{FWE}<0.05) and cluster extent in number of voxel (k)

R right, *L* left

Table 5

Activation foci for the contrast attentional capture > stop

Region		*x*	*y*	*z*	*Z*	*p*	*k*
Sensorimotor cortex							
Precentral gyrus	R	39	−22	64	6.51	<0.001	325
Postcentral gyrus, precentral gyrus, paracentral lobule	L	−33	−28	70	6.40	<0.001	174
Cerebellum							
Cerebellar vermis		0	−52	1	5.19	0.002	40

Local maxima of brain activations during successful attentional capture (ac)–stop in Montreal Neurological Institute (MNI) *x*-, *y*-, and *z*-coordinates with associated *Z*-score ($p_{FWE} < 0.05$) and cluster extent in number of voxel (*k*)

R right, *L* left

Brain Struct Funct. Author manuscript; available in PMC 2016 October 01.

Table 6

Foci of differences in functional connectivity maps for rIFG > rIFJ

Region		*x*	*y*	*z*	*Z*	*k*
Prefrontal cortex						
Inferior frontal gyrus (p. Triangularis)	L	−52	26	14	2.34	32
Middle frontal gyrus	R	42	44	34	3.30	247
Middle frontal gyrus	R	44	4	58	2.13	25
Middle frontal gyrus	L	−36	35	26	2.56	20
Pre-SMA	L	−4	2	68	2.70	42
Precentral gyrus	L	−42	2	50	3.16	165
Anterior cingulate cortex	L	0	20	36	3.94	818
Temporal cortex						
Superior temporal gyrus	R	62	−30	6	3.49	60
Temporal pole	R	44	16	−14	8.13	3,844
Subcortical areas						
Thalamus	L	−8	−24	4	3.38	425
Caudate nucleus[a]	R	12	6	8	6.85	
Pallidum[a]	L	−14	2	0	3.60	
Putamen[a]	L	−24	8	−4	2.88	
Cerebellum						
Cerebellum	R	34	−66	−30	2.76	92
Cerebellum	L	−28	−66	−28	4.78	125

Local maxima of differences in co-activation patterns with rIFG>rIFJ resulting from meta-analytic connectivity modeling in Montreal Neurological Institute (MNI) *x*-, *y*-, and *z*-coordinates with associated *Z*-score and cluster extent in number of voxel (*k*) All reported clusters were derived with a probability of $p>0.95$ for a true difference and an extent threshold of $k = 20$

Pre-SMA pre-supplemental motor area, *R* right, *L* left

[a]Subpeaks of cluster with maximum in temporal pole (44, 16, −14)

Table 7

Foci of differences in functional connectivity maps for rIFJ > rIFG

Region		*x*	*y*	*z*	*Z*	*k*
Prefrontal cortex						
Inferior frontal gyrus (p. Opercularis, p. Triangularis), middle frontal gyrus, precentral gyrus)	R	48	6	16	8.13	1,318
Inferior frontal gyrus (p. Triangularis), middle frontal gyrus	R	48	30	12	2	34
Precentral gyrus	L	−46	2	26	8.13	756
Precentral gyrus	L	−36	−16	56	2.01	7
Parietal cortex						
Superior parietal lobule	R	36	−58	62	2.45	28
Inferior parietal lobule	L	−36	−62	58	3.67	450
Temporal/occipital cortex						
Inferior temporal gyrus	R	46	−60	−10	7.61	820
Superior occipital gyrus, middle occipital gyrus	R	26	−70	44	7.96	850
Fusiform gyrus, inferior occipital gyrus, inferior/middle temporal gyrus	L	−42	−68	−10	7.93	630
Inferior occipital gyrus	R	32	−84	0	4.36	295
Lingual gyrus, inferior/middle occipital gyrus	L	−28	−92	−12	2.56	133

Local maxima of differences in co-activation patterns with rIFJ > rIFG resulting from meta-analytic connectivity modeling in Montreal Neurological Institute (MNI) *x*-, *y*-, and *z*-coordinates with associated *Z*-score and cluster extent in number of voxel (*k*)

All reported clusters were derived with a probability of $p > 0.95$ for a true difference and an extent threshold of $k = 20$

R right, *L* left